Asian Journal of Chemistry; Vol. 38, No. 8 (2026), 2089-2101
ASIAN JOURNAL OF CHEMISTRY
https://doi.org/10.14233/ajchem.2026.36319

Grindstone Assisted Synthesis of Pyrimido-Xanthene Analogues and its Antioxidant, Antidiabetic and Docking Studies

P. LYDIA FESTUS KANMANI[1], S. DURGA DEVI[1], K. PALANISAMY[2] and A. LEEMA ROSE[1,*]

[1]Research Department of Chemistry, Holy Cross College (Affiliated to Bharathidasan University), Tiruchirappalli-620002, India
[2]Research Department of Chemistry, Thanthai Hans Roever College (Affiliated to Bharathidasan University), Perambalur-621220, India

*Corresponding author: E-mail: leemarose25@gmail.com

Received: 27 April 2026 *Accepted*: 30 June 2026 *Published online*: 7 August 2026 AJC-22435

The present study aimed to synthesise a series of pyrimido-xanthene analogues *via* the Biginelli reaction using an eco-friendly grindstone approach and $FeSO_4 \cdot 7H_2O$ as an efficient catalyst. The synthesised compounds were characterized by elemental analysis, FT-IR, ^1H and ^{13}C NMR spectroscopy, and HR-MS. The newly synthesised analogues (**2a-j**) were subsequently evaluated for their antioxidant and antidiabetic activities. Among the tested compounds, analogue **2b** exhibited the most promising antioxidant and antidiabetic potential. Furthermore, molecular docking studies were also performed to gain insights into the binding interactions and inhibition mechanism of the title compounds against the target enzymes.

Keywords: Antidiabetic, Antioxidant, Grindstone, Molecular docking, Pyrimidine, Xanthene.

INTRODUCTION

Heterocyclic compounds such as pyrimidines and xanthenes occupy an important position in medicinal chemistry due to their structural diversity, broad therapeutic profile and synthetic accessibility [1]. Pyrimidine represents one of the fundamental building blocks of nucleic acids and is present in both DNA and RNA. Structural modification of the pyrimidine nucleus has generated compounds with significant pharmacological properties, particularly in diabetes management. Pyrimidine derivatives and dihydropyrimidines (DHPMs) have been identified as selective α-glucosidase inhibitors and are regarded as promising candidates for antidiabetic drug development [2].

Growing environmental concerns have encouraged the adoption of green synthetic methodologies as alternatives to conventional chemical processes. Such approaches rely on environmentally benign solvents and catalysts for the reducing energy consumption and waste generation [3]. Green chemistry principles favour shorter reaction sequences, lower process mass intensity and improved resource utilisation, making the preparation of bioactive molecules both economically attractive and environmentally responsible [4].

The search for sustainable synthetic technologies has directed considerable attention toward multicomponent reactions (MCRs). These reactions offer high atom economy, operational simplicity, reduced purification requirements and minimal byproduct formation. Their utility in the preparation of medicinally important compounds has led to widespread application in academic and industrial research laboratories [5].

Among the various multicomponent reaction (MCR) strategies, the Biginelli reaction remains one of the most widely investigated methods for constructing pyrimidine-containing heterocycles. Interest in this transformation originated from the discovery of nifedipine-type calcium channel blockers derived from the Biginelli scaffold [6]. Subsequent investigations established antioxidant, anti-Alzheimer, antiviral, antibacterial, anti-inflammatory, analgesic and anticancer properties for these compounds [7-14]. Pyrimidines possess electron rich heterocyclic frameworks and serve as essential constituents of genetic material, reinforcing their biological significance [12]. Their interaction with carbohydrate-metabolising enzymes has strengthened interest in pyrimidine derivatives as antidiabetic agents. Representative pyrimidine-based antidiabetic drugs are presented in Fig. 1.

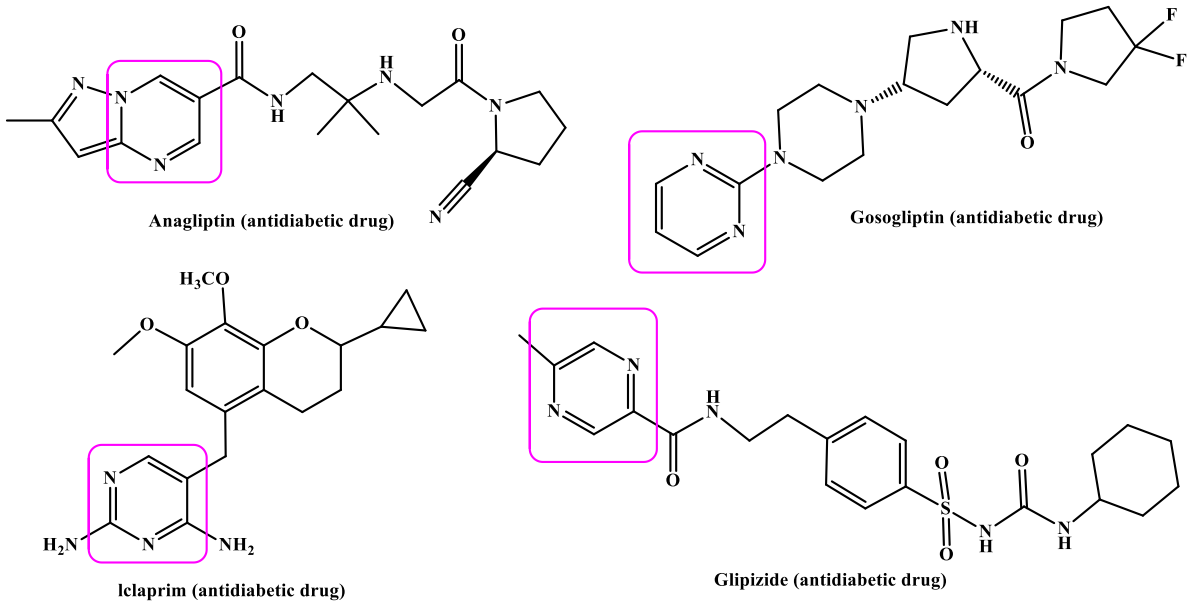

Fig. 1. Commercially available antidiabetic drugs containing pyrimidine derivatives

Xanthenes constitute a distinct class of oxygen containing tricyclic heterocycles with diverse biological applications [15,16]. Structural modification at the C-9 position exerts a strong influence on their physico-chemical and pharmacological properties. Xanthydrol, xanthene-9-carboxylic acid and related derivatives have exhibited neuroprotective, antidiabetic, antibacterial and cytotoxic activities [17]. Xanthene analogues have also been associated with analgesic, antiviral, anti-inflammatory, antioxidant, antibacterial and anticancer effects [18]. Their structural resemblance to mangiferin, a naturally occurring secondary metabolite used in diabetes management, supports their potential as antidiabetic pharmacophores [19]. Selected biologically active xanthene derivatives are illustrated in Fig. 2.

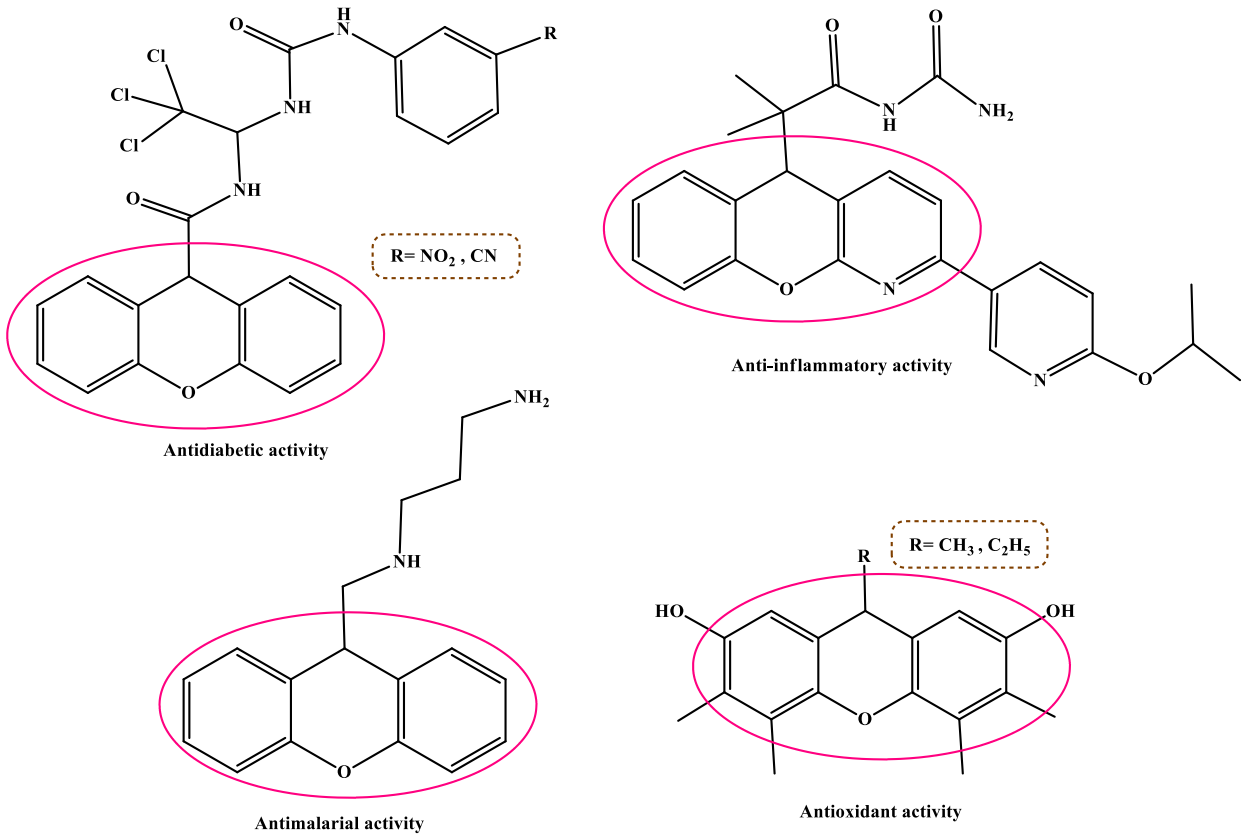

Fig. 2. Biologically active xanthene derivatives

Continuous research on pyrimidine and xanthene chemistry has produced numerous biologically active compounds; however, hybrids incorporating both pharmacophores remain limited. Combining these privileged scaffolds may enhance biological activity through complementary interactions. Moreover, many existing synthetic methods for related heterocycles employ hazardous solvents, prolonged reaction times, or expensive catalysts, limiting their practicality and sustainability. The present investigation addresses these limitations through the development of a grindstone-assisted, solvent-free synthetic protocol employing $FeSO_4·7H_2O$ as efficient catalyst for the synthesis of novel pyrimido-xanthene derivatives (**2a-j**). The synthesised compounds were subjected to antioxidant and antidiabetic evaluation to explore the therapeutic potential of this hybrid scaffold while establishing a greener alternative to conventional synthetic methodologies.

EXPERIMENTAL

All chemicals and solvents were procured from commercial suppliers and used as received without further purification. Melting points were measured using open capillary tubes and are not corrected. FT-IR spectra using KBr pellets were recorded on a Shimadzu 8201PC spectrophotometer in the range of 4000-400 cm^{-1}. The ^1H and ^{13}C NMR spectra were obtained using a JEOL 400 MHz spectrometer. Elemental analyses (CHN) were carried out on a Varian EL III elemental analyzer. The purity of the synthesised compounds was monitored by thin-layer chromatography (TLC) using silica gel plates.

General synthesis of pyrimido-xanthene *via* Biginelli reaction (2a-g): Xanthene (0.004 mol, 1.16 g), guanidine hydrochloride (0.004 mol, 0.38 g), vanillin (0.004 mol, 0.60 g) and $FeSO_4·7H_2O$ as catalyst were thoroughly mixed in a mortar using a pestle under grindstone conditions. The progress of the reaction was monitored by TLC. Upon completion of the reaction, the reaction mixture was poured into ice-cold water, resulting in the formation of a yellow precipitate. The obtained solid product was filtered, dried and recrystallised from hot ethanol (**Scheme-I**).

2-Amino-4-(2-hydroxy-4-methoxyphenyl)-12-phenyl-2,3,4,5,6,12-hexahydro-1*H*-chromeno[2,3-*h*]quinazolin-9-ol (2a): Yield: 98%; yellow solid; m.p.: 242 ºC; Elemental anal. of $C_{28}H_{27}N_3O_4$: calcd (found) %: C, 71.62 (71.60); H, 5.80 (5.82); N, 8.95 (8.94). IR (KBr, ν_{max}, cm^{-1}): 3386 (OH), 3117 (NH *str*.), 2992 (Ar-CH *str*.), 1375 (C-N-C *str*.), 1086 (C-O-C); ^1H NMR (400 MHz, $CDCl_3$, δ ppm): 12.30 (2H, s, OH), 10.80 (2H, s, NH), 8.82-7.93 (3H, m, vanillin, *J* = 7.2 Hz), 7.40-7.27 (5H, m, Ar-H, *J* = 7.7 Hz), 7.20-6.06 (3H, m, phenyl ring, *J* = 7.2 Hz), 5.60 (2H, s, NH_2), 4.89 (1H, s, CH-NH_2), 4.42 (1H, s, CH-vanillin), 3.83 (3H, s, OCH_3), 3.42 (1H, s, CH-Ph), 2.60-1.72 (4H, m, CH_2); ^{13}C NMR (400 MHz, $CDCl_3$, δ ppm): 152.5, 147.6, 142.4, 142.1, 141.3, 129.2, 128.2, 127.8, 127.0, 126.2, 121.8, 119.2, 110.6, 109.9, 89.6, 52.6, 42.6, 26.1; HR-MS (relative intensity %): *m/z* 469.53 (M^+, 31.5%).

2-Amino-4-(3-nitrophenyl)-12-phenyl-2,3,4,5,6,12-hexahydro-1*H*-chromeno[2,3-*h*]quinazolin-9-ol (2b): Yield: 90%; pale yellow solid; m.p.: 220 ºC; Elemental anal. of $C_{27}H_{24}N_4O_4$: calcd. (found) %: C, 69.22 (69.20); H, 5.16 (5.14); N, 11.96 (11.94). IR (KBr, ν_{max}, cm^{-1}): 3267 (OH), 3112 (NH *str*.), 2977 (Ar-CH *str*.), 1478 (NO_2 *str*.), 1338 (C-N-C *str*.), 1071 (C-O-C); ^1H NMR (400 MHz, $CDCl_3$, δ ppm): 12.31 (2H, s, OH), 10.81 (2H, s, NH), 8.12-7.57 (4H, m, phenyl ring, *J* = 7.4 Hz), 7.40-7.27 (5H, m, Ar-H, *J* = 7.6 Hz), 7.23-6.19 (3H, m, phenyl ring, *J* = 7.3 Hz), 5.62 (2H, s, NH_2), 4.89 (1H, s, CH-NH_2), 3.42 (1H, s, CH-Ph), 2.60-1.71 (4H, m, CH_2); ^{13}C NMR (400 MHz, $CDCl_3$, δ ppm): 162.1, 154.5, 147.7, 143.4, 141.1, 139.2, 130.1, 129.8, 127.0, 126.4, 123.5, 121.5, 119.4, 113.1, 110.6, 90.2, 41.6, 26; HR-MS (relative intensity %): *m/z* 468.18 (M^+, 30.8%).

2-Amino-4,12-diphenyl-2,3,4,5,6,12-hexahydro-1*H*-chromeno[2,3-*h*]quinazolin-9-ol (2c): Yield: 94%; yellowish-white solid; m.p.: 260 ºC; Elemental anal. of $C_{27}H_{25}N_3O_2$: calcd. (found) %: C, 76.57 (76.60); H, 5.95 (5.92); N, 9.92 (9.94).IR (KBr, ν_{max}, cm^{-1}): 3254 (OH), 3117 (NH *str*.), 2977 (Ar-CH *str*.), 1310 (C-N-C *str*.), 1076 (C-O-C); ^1H NMR (400 MHz, $CDCl_3$, δ ppm): 12.36 (1H, s, OH), 10.83 (2H, s, NH), 7.40-7.29 (5H, m, Ar-H, *J* = 7.8 Hz), 7.34-7.25 (5H, m, Ar-H, *J* = 7.3 Hz),7.20-6.18 (3H, m, phenyl ring, *J* = 7.2 Hz), 5.63 (2H, s, NH_2), 4.89 (1H, s, CH-NH_2), 4.71 (1H, s, CH-Ph), 4.54 (1H, s, CH-NH), 2.61-1.78 (4H, m, CH_2); ^{13}C NMR (400 MHz, $CDCl_3$, δ ppm): 147.6, 142.4, 141.3, 138.2, 129.2, 128.4, 128.2, 127.8, 127.2, 127.0, 126.2, 121.8, 119.2, 113.3, 109.9, 89.6, 42.6, 26.1; HR-MS (relative intensity %): *m/z* 424.20 (M^+, 29.6%).

2-Amino-4-(2-hydroxyphenyl)-12-phenyl-2,3,4,5,6,12-hexahydro-1*H*-chromeno[2,3-*h*]quinazolin-9-ol (2d): Yield: 93%; light brown solid; m.p.: 210 ºC; Elemental anal. of $C_{27}H_{25}N_3O_3$: calcd. (found) %: C, 73.78 (73.75); H, 5.73 (5.76); N, 9.56 (9.58); IR (KBr, ν_{max}, cm^{-1}): 3251 (OH), 3119 (NH *str*.), 2933 (Ar-CH *str*.), 1389 (C-N-C *str*.), 1034 (C-O-C); ^1H NMR (400 MHz, $CDCl_3$, δ ppm): 12.34 (2H, s, OH), 10.83 (2H, s, NH), 7.42-7.29 (5H, m, Ar-H, *J* = 7.7 Hz), 7.35-6.89 (4H, m, Ph-CH, *J* = 7.0 Hz), 7.20-6.08 (3H, m, phenyl ring, *J* = 7.2 Hz), 5.64 (2H, s, NH_2), 4.89 (1H, s, CH-NH_2), 4.62 (1H, s, CH-NH), 3.42 (1H, s, CH-Ph), 2.64-1.72 (4H, m, CH_2); ^{13}C NMR (400 MHz, $CDCl_3$, δ ppm): 155.1, 147.6, 142.4, 141.2, 130.3, 129.2, 128.3, 127.1, 126.4, 121.5, 119.2, 118.6, 109.5, 89.6, 42.4, 26.3; HR-MS (relative intensity %): *m/z* 440.19 (M^+, 30.4%).

2-Amino-4-(4-(dimethylamino)phenyl)-12-phenyl-2,3,4,5,6,12-hexahydro-1*H*-chromeno[2,3-*h*]quinazolin-9-ol (2e): Yield: 94%; dull-white solid; m.p.: 216 ºC; Elemental anal. of $C_{29}H_{30}N_4O_2$: calcd. (found) %: C, 74.65 (74.62); H, 6.48 (6.45); N, 12.01 (12.03); IR (KBr, ν_{max}, cm^{-1}): 3332 (OH), 3112 (NH *str*.), 2921 (Ar-CH *str*.), 1370 (C-N-C *str*.), 1043 (C-O-C); ^1H NMR (400 MHz, $CDCl_3$, δ ppm): 12.35 (1H, s, OH), 10.84 (2H, s, NH), 7.43-7.29 (5H, m, Ar-H, *J* = 7.6 Hz), 7.25-6.05 (3H, m, phenyl ring, *J* = 7.3 Hz), 7.15-6.19 (4H, d, *p*-aminophenyl, *J* = 7.1 Hz), 5.60 (2H, s, NH_2), 4.87 (1H, s, CH-NH_2), 4.63 (1H, s, CH-NH), 4.08 (6H, s, $N(CH_3)_2$), 3.42 (1H, s, CH-Ph), 2.60-1.71 (4H, m, CH_2); ^{13}C NMR (400 MHz, $CDCl_3$, δ ppm): 149.4, 147.6, 142.4, 141.3, 129.2, 128.1, 127.8, 127.6, 127.0, 126.5, 126.3, 121.8, 119.2, 112.7, 110.3, 109.1, 89.6, 42.6, 26.1, 20.4; HR-MS (relative intensity %): *m/z* 467.24 (M^+, 31.8%).

2-Amino-4-(4-chlorophenyl)-12-phenyl-2,3,4,5,6,12-hexahydro-1*H*-chromeno[2,3-*h*]quinazolin-9-ol (2f): Yield: 92%; light yellow solid; m.p.: 264 ºC; Elemental anal. of

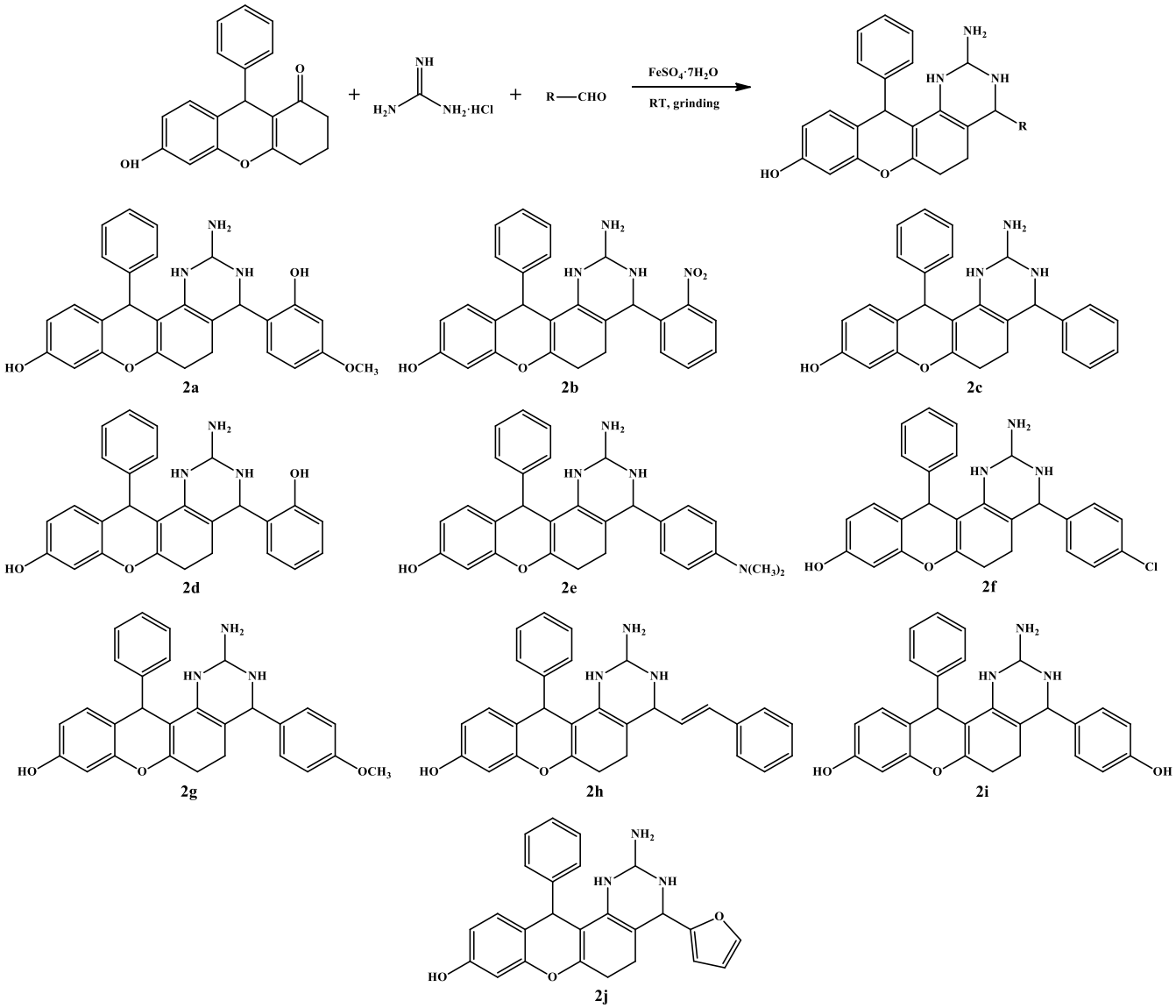

Scheme-I: Synthetic route of proposed compound **2a-j**

$C_{27}H_{24}ClN_3O_2$: calcd. (found) %: C, 70.81 (70.83); H, 5.28 (5.30); N, 9.18 (9.15); IR (KBr, ν_{max}, cm^{-1}): 3304 (OH), 3122 (NH *str.*), 2987 (Ar-CH *str.*), 1380 (C-N-C *str.*), 1086 (C-O-C), 759 (C-Cl); ^{1}H NMR (400 MHz, $CDCl_3$, δ ppm): 12.34 (1H, s, OH), 10.82 (2H, s, NH), 7.45-7.32 (4H, dd, Cl-Ph, *J* = 7.4 Hz), 7.28-7.10 (5H, m, Ar-H, *J* = 7.2 Hz), 6.85-6.10 (2H, d, phenyl ring, *J* = 7.0 Hz), 6.38 (1H, s, Ph-CH), 5.60 (2H, s, NH_2), 4.89 (1H, s, CH-NH_2), 4.74 (1H, s, CH), 4.56 (1H, s, CH-NH), 2.63-1.70 (4H, m, CH_2); ^{13}C NMR (400 MHz, $CDCl_3$, δ ppm): 162.5, 154.1, 147.6, 141.3, 136.0, 132.6, 130.3, 129.2, 128.3, 127.1, 126.2, 121.8, 119.2, 113.3, 110.6, 89.6, 42.6, 26.1; HR-MS (relative intensity %): *m/z* 459.15 (M^+, 32.0%).

2-Amino-4-(4-methoxyphenyl)-12-phenyl-2,3,4,5,6,12-hexahydro-1*H*-chromeno[2,3-*h*]quinazolin-9-ol (2g): Yield: 96%; white solid; m.p.: 285 ºC; Elemental anal. of $C_{28}H_{27}N_3O_3$: calcd. (found) %: C, 74.15 (74.10); H, 6.00 (6.03); N, 9.27 (9.24); IR (KBr, ν_{max}, cm^{-1}): 3407 (OH), 2921 (NH *str.*), 2856 (Ar-CH *str.*), 1450 (C-N-C *str.*), 1029 (C-O-C); ^{1}H NMR (400 MHz, $CDCl_3$, δ ppm): 12.33 (1H, s, OH), 10.84 (2H, s, NH), 7.40-7.25 (5H, m, Ar-H, *J* = 7.8 Hz), 7.20-6.06 (3H, m, phenyl ring, *J* = 7.4 Hz), 7.11-6.85 (4H, m, OCH_3-Ph *J* = 7.3 Hz), 5.60 (2H, s, NH_2), 4.89 (1H, s, CH-NH_2), 4.73 (1H, s, Ar-CH), 3.85 (3H, s, OCH_3), 3.42 (1H, s, CH-Ph), 2.60-1.73 (4H, m, CH_2); ^{13}C NMR (400 MHz, $CDCl_3$, δ ppm): 158.5, 147.6, 142.5, 141.1, 130.4, 129.2, 128.3, 127.0, 126.4, 121.8, 119.2, 114.1, 113.3, 110.2, 109.1, 52.6, 42.6, 26.1; HR-MS (relative intensity %): *m/z* 454.21 (M^+, 30.7%).

2-Amino-12-phenyl-4-((*E*)-styryl)-2,3,4,5,6,12-hexahydro-1*H*-chromeno[2,3-*h*]quinazolin-9-ol (2h): Yield: 90%; yellow solid; m.p.: 215 ºC; Elemental anal. of $C_{29}H_{27}N_3O_2$: calcd. (found) %: C, 77.48 (77.46); H, 6.05 (6.07); N, 9.35 (9.37); IR (KBr, ν_{max}, cm^{-1}): 3258 (OH), 3112 (NH *str.*), 2982 (Ar-CH *str.*), 1323 (C-N-C *str.*), 1095 (C-O-C); ^{1}H NMR (400 MHz, $CDCl_3$, δ ppm): 12.36 (1H, s, OH), 10.83 (2H, s, NH), 7.40-7.26 (5H, m, Ph, *J* = 7.1 Hz), 7.35-7.22 (5H, m, Ar-H, *J* = 7.3 Hz), 7.20-6.06 (3H, m, phenyl ring, *J* = 7.2 Hz), 6.39-6.19 (2H, d, CH=CH), 5.60 (2H, s, NH_2), 4.89 (1H, s, CH-NH_2), 4.73 (1H, s, Ar-CH), 3.42 (1H, s, CH-Ph), 2.64-

1.70 (4H, m, CH_2); ^{13}C NMR (400 MHz, $CDCl_3$, δ ppm): 147.6, 142.3, 141.3, 136.4, 129.5, 129.2, 128.6, 127.0, 126.8, 126.4, 123.3, 121.2, 119.9, 119.2, 113.3, 109.9, 89.6, 42.6, 26.1. HR-MS (relative intensity %): *m/z* 449.54 (M^+, 32.5%).

2-Amino-4-(4-hydroxyphenyl)-12-phenyl-2,3,4,5,6,12-hexahydro-1*H*-chromeno[2,3-*h*]quinazolin-9-ol (2i): Yield: 93%; pale yellowish brown solid; m.p.: 256 ºC; Elemental anal. of $C_{27}H_{25}N_3O_3$: calcd. (found) %: C, 73.78 (73.71); H, 5.73 (5.70); N, 9.56 (9.54); IR (KBr, ν_{max}, cm^{-1}): 3393 (OH), 3076 (NH *str.*), 2954 (Ar-CH *str.*), 1370 (C-N-C *str.*), 1071 (C-O-C); ^{1}H NMR (400 MHz, $CDCl_3$, δ ppm): 12.31 (2H, s, OH), 10.81 (2H, s, NH), 7.62-7.27 (5H, m, Ar-H, *J* = 7.9 Hz), 7.33-6.89 (4H, m, Ph-CH, *J* = 7.4 Hz), 7.23-6.19 (3H, m, phenyl ring, *J* = 7.2 Hz), 5.62 (2H, s, NH_2), 4.89 (1H, s, CH-NH_2), 4.60 (1H, s, CH-NH), 3.42 (1H, s, CH-Ph), 2.60-1.71 (4H, m, CH_2); ^{13}C NMR (400 MHz, $CDCl_3$, δ ppm): 155.1, 147.6, 142.4, 141.2, 130.3, 129.2, 128.3, 127.1, 126.4, 121.5, 119.2, 118.6, 109.5, 89.6, 42.4, 26.3; HR-MS (relative intensity %): *m/z* 440.19 (M^+, 30.4%).

2-Amino-4-(furan-2-yl)-12-phenyl-2,3,4,5,6,12-hexahydro-1*H*-chromeno[2,3-*h*]quinazolin-9-ol (2j): Yield: 91%; white solid; m.p.: 263 ºC; Elemental anal. of $C_{25}H_{23}N_3O_3$: calcd. (found) %: C, 72.62 (72.60); H, 5.61 (5.65); N, 10.16 (10.14); IR (KBr, ν_{max}, cm^{-1}): 3421 (OH), 3066 (NH *str.*), 2940 (Ar-CH *str.*), 1380 (C-N-C *str.*), 1142 (C-O-C); ^{1}H NMR (400 MHz, $CDCl_3$, δ ppm): 12.34 (1H, s, OH), 10.85 (2H, s, NH), 7.65-6.26 (3H, m, furyl, *J* = 7.5 Hz), 7.36-7.27 (5H, m, Ar-H, *J* = 7.7 Hz), 7.20-6.20 (3H, m, phenyl ring, *J* = 7.2 Hz), 5.63 (2H, s, NH_2), 4.89 (1H, s, CH-NH_2), 4.73 (1H, s, Ar-CH), 3.42 (1H, s, CH-Ph), 2.93-1.74 (4H, m, CH_2); ^{13}C NMR (400 MHz, $CDCl_3$, δ ppm): 152.5, 147.6, 142.4, 142.1, 141.3, 129.2, 128.7, 127.4, 127.0, 126.6, 126.2, 121.8, 119.2, 113.3, 110.6, 109.9, 89.6, 42.6, 26.1; HR-MS (relative intensity %): *m/z* 414.18 (M^+, 24.4%).

Antioxidant studies

DPPH scavenging assay: The antioxidant potential of the synthesised compounds was evaluated using the DPPH free radical scavenging assay. The reduction in the characteristic violet colour of DPPH reflects the radical scavenging ability of the tested compounds and is directly proportional to their antioxidant activity. The assay was carried out according to the method reported by Aroua *et al.* [20]. Briefly, 1 mL of DMSO solutions of the test compounds (final concentration: 1 mM) was mixed with DPPH solution prepared in DMSO at concentrations ranging from 125 to 500 µM. The reaction mixtures were incubated at 37 ºC for 30 min, and the decrease in absorbance was measured spectrophotometrically at 517 nm.

FRAP assay: The ferric reducing antioxidant power (FRAP) assay was performed according to the reported method [21]. The FRAP reagent was freshly prepared by mixing $FeCl_3 \cdot 6H_2O$ (20 mM), TPTZ solution (10 mM in 40 mM HCl) and acetate buffer (300 mM, pH 3.6) in a ratio of 1:1:10. An aliquot of the test sample (0.1 mL, final concentration 1 mM in DMSO) was added to 2 mL of the FRAP reagent and incubated at 37 ºC for 30 min. The absorbance was recorded at 593 nm using a UV-Visible spectrophotometer.

Antidiabetic effect

α-Amylase inhibitory action: The α-amylase inhibitory activity of the synthesised compounds was evaluated according to the reported procedure [20]. Briefly, 500 µL of the test sample (125-500 µM) was pre-incubated with 500 µL of α-amylase solution (0.5 mg/mL, *A. oryzae*) prepared in 0.2 M phosphate buffer for 10 min at 25 ºC. Following pre-incubation, 500 µL of 1% starch solution prepared in 0.02 M sodium phosphate buffer was added and the reaction mixture was incubated for an additional 10 min at 25 ºC. The reaction was terminated by the addition of 1 mL of 3,5-dinitrosalicylic acid (DNS) reagent, followed by heating in a boiling water bath for 5 min. After cooling to room temperature, the reaction mixture was diluted with 10 mL of distilled water and the absorbance was measured at 540 nm. Acarbose was employed as the reference standard for comparison of inhibitory activity [22]. The % of enzyme inhibition was determined using the below relation:

$$\text{α-Amylase inhibitory effect (\%)} = \frac{A_{control} - A_{compound}}{A_{control}} \times 100 \quad (1)$$

α-Glucosidase inhibitory action: The α-glucosidase inhibitory activity was evaluated using a modified version of a previously reported method [23]. Briefly, 1 mg of α-glucosidase and 100 mg of bovine serum albumin (BSA) were dissolved in 50 mL of phosphate buffer. The reaction mixture consisted of 5 µL of the test samples at different concentrations (125-1000 µM), 250 µL of 5 mM *p*-nitrophenyl-α-D-glucopyranoside (pNPG) as the substrate and 490 µL of phosphate buffer. After pre-incubation at 37 ºC for 5 min, 200 µL of the α-glucosidase enzyme solution was added and the mixture was incubated at 37 ºC for 15 min. The reaction was terminated by adding 1000 µL of 100 mM Na_2CO_3. The enzymatic activity was determined by measuring the absorbance at 400 nm using a UV-Vis spectrophotometer. Acarbose was used as the positive control (standard α-glucosidase inhibitor) [24]. The percentage inhibition of α-glucosidase activity was calculated using the following equation:

$$\text{α-Glucosidase activity (\%)} = \frac{A_{control} - A_{compound}}{A_{control}} \times 100 \quad (1)$$

Statistical analysis: All experiments were performed in triplicate and the results are expressed as mean ± standard deviation (SD). Statistical analyses were carried out using Microsoft Excel (Microsoft Corporation, Redmond, WA, USA). The IC_{50} values were determined from plots of percentage inhibition *versus* logarithm of concentration using linear regression analysis of the dose–response data. The concentration corresponding to 50% inhibition was calculated from the regression equation. The goodness of fit of the regression model was evaluated using the coefficient of determination (R^2). The statistical significance was considered at $p < 0.05$.

***In silico* Docking studies:** Molecular docking studies were performed to investigate the binding interactions of the synthesised pyrimido-xanthene derivatives (**2a-j**) with the target proteins 2F6D, 2QV4 and 3MNG and to predict their preferred binding orientations within the active sites. The three-dimen-

sional structures of the target proteins were retrieved from the Protein Data Bank (PDB). Co-crystallized ligands and water molecules were removed prior to docking calculations. Polar hydrogen atoms and Gasteiger charges were assigned using AutoDockTools (ADT) version 1.5.2 and the prepared protein structures were converted into PDBQT format [25,26]. The docking grids were generated using ADT. For protein 2F6D, the grid center was defined at x = 10.945 Å, y = 8.351 Å and z = -9.511 Å with dimensions of 24 × 24 × 24 grid points. For 2QV4, the grid center coordinates were x = 10.721 Å, y = 48.233 Å and z = 20.805 Å with a grid size of 24 × 24 × 24 points. The grid for 3MNG was centered at x = 8.341 Å, y = 45.637 Å and z = 30.621 Å with dimensions of 18 × 18 × 18 grid points. A grid spacing of 1.0 Å was employed for all docking calculations. The ligand structures were energy-minimized using the conjugate gradient AMMP method implemented in the VEGA ZZ software package [27]. The optimized ligand structures were converted from PDB to PDBQT format using ADT. Molecular docking simulations were carried out using AutoDock Vina with an exhaustiveness value of 8 [28]. The resulting binding conformations were analyzed using ADT, while ligand–protein interactions were visualized and interpreted using Discovery Studio Visualizer [29].

RESULTS AND DISCUSSION

A series of novel pyrimido-xanthene derivatives (**2a-j**) were synthesised through a grindstone-assisted, solvent-free Biginelli reaction using $FeSO_4 \cdot 7H_2O$ as an efficient catalyst. The structures of all the synthesised derivatives **2a-j** were successfully established by FT-IR, ^1H & ^{13}C NMR and HR-MS analyses. The FT-IR spectra exhibited characteristic absorption bands in the 3421-3258, 3122-3066, 2992-2856, 1450-1310 and 1095-1034 cm^{-1} region corresponds to O–H, N–H, aromatic C–H, C–N–C and C–O–C stretching vibrations, respectively. The absence of aldehydic carbonyl and aldehydic C–H absorptions associated with the starting aldehydes, together with the appearance of characteristic C–N–C vibrations of the pyrimidine ring and C–O–C stretching bands of the xanthene framework, confirms the successful cyclocondensation leading to the target fused heterocyclic systems. The ^1H NMR spectra of compounds **2a-j** displayed broad singlets in the region δ 12.34-12.30 ppm attributable to hydroxyl protons and signals at δ 10.86-10.80 ppm assigned to N–H protons. The broad nature of these resonances arises from hydrogen-bonding interactions and proton-exchange processes commonly observed for exchangeable protons. Aromatic proton resonances appeared as overlapping multiplets distributed over narrow chemical shift ranges owing to the extended conjugation and fused nature of the pyrimido-xanthene framework. Similar chemical shifts among the derivatives may originate from the combined influence of substituent effects, electron delocalisation, ring-current contributions and conformational averaging within the heterocyclic system. The ^{13}C NMR spectra displayed characteristic resonances at δ 152.5, 89.6 and 26.3-26.0 ppm, assigned to the C=N carbon of the pyrimidine moiety, methine carbon attached to the amino functionality and methylene carbons of the xanthene skeleton, respectively. In several derivatives, the number of observed carbon resonances was lower than the total number of carbon atoms present in the molecular structure. Such behaviour can be attributed to chemically equivalent carbon atoms arising from molecular symmetry, overlap of aromatic carbon signals within restricted spectral regions and the inherently lower sensitivity of certain quaternary carbons. Similar spectral features are frequently encountered in highly substituted aromatic and fused heterocyclic systems [30].

Antioxidant assessment

DPPH assay: Table-1 presents the DPPH scavenging activity of the synthesised xanthene analogues **2a-j**. The compounds exhibited enhanced DPPH scavenging activity in the concentration range of 120-500 μM compared with the standard, ascorbic acid; however, at 1000 μM, ascorbic acid demonstrated superior activity. The DPPH scavenging activity of compounds **2a-j** increased with increasing concentration, indicating a clear dose-dependent response. Among the tested derivatives, compounds **2c**, **2e** and **2j** displayed significant antioxidant activity with IC_{50} values of 112.23, 94.06 and 129.40 μM, respectively. Compound **2e** exhibited the highest DPPH scavenging activity (IC_{50} = 94.06 μM), surpassing both the other synthesised analogues and the standard ascorbic acid (IC_{50} = 131.89 μM). In contrast, compound **2a** showed the weakest antioxidant activity, with an IC_{50} value of 413.79 μM. The DPPH assay is based primarily on the ability of antioxidants to donate hydrogen atoms or electrons to neutralise

TABLE-1
DPPH RADICAL SCAVENGING ACTION OF COMPOUNDS **2a-j**

Compound	Scavenging activity (%)				IC_{50} (μM)
	125 μM	250 μM	500 μM	1000 μM	
2a	22.3 ± 1.2	43.4 ± 2.3	66.3 ± 1.7	81.8 ± 2.5	413.79
2b	46.6 ± 1.2	60.0 ± 0.8	86.0 ± 2.8	95.0 ± 3.0	237.08
2c	42.8 ± 1.5	62.4 ± 2.3	79.5 ± 0.3	97.4 ± 2.8	112.23
2d	47.3 ± 0.7	78.5 ± 1.8	91.8 ± 3.2	95.5 ± 1.3	160.93
2e	50.4 ± 2.6	71.6 ± 2.4	79.0 ± 1.3	92.6 ± 2.3	94.06
2f	32.8 ± 1.2	50.4 ± 2.9	92.6 ± 0.4	95.4 ± 3.6	213.14
2g	46.1 ± 2.9	78.2 ± 1.7	84.3 ± 3.4	91.3 ± 0.7	148.14
2h	37.2 ± 0.8	54.8 ± 2.2	85.2 ± 0.6	97.0 ± 1.5	185.46
2i	38.5 ± 2.3	47.6 ± 1.6	73.8 ± 2.4	84.5 ± 1.8	257.13
2j	37.2 ± 2.8	67.0 ± 1.7	76.9 ± 3.1	93.8 ± 1.2	129.40
Ascorbic acid	40.5 ± 0.5	61.2 ± 2.8	78.2 ± 1.6	91.8 ± 2.2	131.89

free radicals, with lower IC_{50} values indicating stronger antioxidant potential.

FRAP assay: Table-2 presents the comparative FRAP antioxidant capacities of the synthesised analogues **2a-j** with reference to ascorbic acid. The ferric reducing antioxidant power of compounds **2a-j** increased with increasing concentration, reflecting a dose-dependent response. Most of the synthesised derivatives displayed appreciable ferric reducing activity with IC_{50} values ranging from 147.11 to 238.91 μM, whereas compounds **2a** and **2f** exhibited lower activity with IC_{50} values of 350.18 and 303.31 μM, respectively, compared with ascorbic acid (IC_{50} = 241.69 μM). Compounds **2e** and **2h**, bearing electron-donating substituents on the benzene ring, exhibited the strongest ferric reducing activity, with IC_{50} values of 147.11 and 160.79 μM, respectively, and ranked among the most active derivatives in the series. In contrast, compounds **2a** and **2f** displayed comparatively weak FRAP activity. The FRAP assay measures the electron-donating ability of antioxidants through the reduction of Fe^{3+} to Fe^{2+}, with lower IC_{50} values corresponding to greater reducing potential and antioxidant capacity.

Antidiabetic activity

α-Glucosidase assay: The inhibitory effects of analogues **2a-j** against α-glucosidase were evaluated. The synthesised compounds exhibited varying degrees of α-glucosidase inhibition, with IC_{50} values ranging from 135.57 to 180.32 μM for the more active derivatives (Table-3). Compounds **2b** and **2d** emerged as the most potent α-glucosidase inhibitors in the series, with IC_{50} values of 135.57 and 145.49 μM, respectively and exhibited stronger inhibitory activity than the reference drug acarbose. Compound **2g** displayed the weakest antidiabetic potential, with an IC_{50} value of 428.17 μM.

α-Amylase assay: Table-4 summarizes the α-amylase inhibitory activity of compounds **2a-j**. The results showed that the synthesised derivatives possessed stronger inhibitory activity than the reference drug acarbose in several cases. Enzyme inhibition increased with increasing concentration, confirming a concentration-dependent response. Most compounds exhibited appreciable antidiabetic potential, whereas compounds **2a**, **2f**, **2g** and **2j** displayed weaker activity with IC_{50} values of 409.22, 354.17, 325.06 and 283.00 μM, respectively. Compound **2b** emerged as the most active derivative in the series, with an IC_{50} value of 141.46 μM, compared with acarbose (IC_{50} = 220.83 μM). Compound **2a** exhibited the lowest α-amylase inhibitory activity, with an IC_{50} value of 409.22 μM.

Docking studies

Antidiabetic

α-Glucosidase inhibition: Docking studies were carried out to obtain deeper insight into the possible mechanism underlying the biological activity of the synthesised compounds.

TABLE-2
ANTIOXIDANT ACTIVITY OF COMPOUNDS **2a-j** THROUGH FRAP ASSAY

Compound	Scavenging activity (%)				IC_{50} (μM)
	125 μM	250 μM	500 μM	1000 μM	
2a	24.6 ± 1.4	46.2 ± 2.3	71.7 ± 1.3	91.8 ± 2.2	350.18
2b	29.0 ± 1.6	46.7 ± 2.5	82.6 ± 1.4	97.0 ± 2.3	285.80
2c	34.6 ± 2.4	61.3 ± 1.6	84.9 ± 2.1	94.8 ± 1.2	162.35
2d	38.9 ± 1.1	54.6 ± 2.4	72.9 ± 1.1	91.7 ± 2.3	214.59
2e	36.8 ± 2.2	69.0 ± 1.7	70.6 ± 2.4	95.0 ± 1.3	147.11
2f	24.7 ± 2.3	47.0 ± 0.7	84.8 ± 2.2	90.7 ± 1.3	303.31
2g	33.4 ± 1.6	55.1 ± 0.9	87.0 ± 1.5	91.4 ± 2.6	197.76
2h	39.0 ± 2.3	56.2 ± 1.8	85.1 ± 2.9	95.2 ± 1.8	160.79
2i	41.2 ± 1.8	58.4 ± 2.6	73.0 ± 1.3	89.4 ± 2.2	163.97
2j	36.9 ± 1.1	58.7 ± 2.3	64.6 ± 1.4	95.0 ± 2.2	238.91
Ascorbic acid	29.1 ± 2.9	51.4 ± 0.6	89.2 ± 2.8	95.1 ± 1.9	241.69

TABLE-3
ANTIDIABETIC EFFECT OF COMPOUNDS **2a-j** THROUGH α-GLUCOSIDASE INHIBITION ASSAY

Compound	Inhibition rate (%)				IC_{50} (μM)
	125 μM	250 μM	500 μM	1000 μM	
2a	26.3 ± 2.8	46.1 ± 1.9	84.0 ± 0.5	92.3 ± 1.7	300.74
2b	32.0 ± 2.3	66.0 ± 1.3	86.4 ± 2.6	90.0 ± 1.8	135.57
2c	22.0 ± 2.3	42.1 ± 1.9	78.4 ± 2.6	94.1 ± 0.9	353.52
2d	38.0 ± 2.7	62.3 ± 0.7	74.1 ± 2.9	84.2 ± 1.8	145.49
2e	34.0 ± 1.5	68.2 ± 2.8	68.6 ± 1.4	82.2 ± 2.8	158.66
2f	28.0 ± 1.3	40.3 ± 2.7	62.4 ± 1.6	86.0 ± 2.5	404.47
2g	18.6 ± 2.4	43.9 ± 1.1	66.2 ± 2.8	81.9 ± 1.1	428.17
2h	36.5 ± 1.5	60.1 ± 2.9	71.9 ± 1.1	92.0 ± 0.6	201.57
2i	30.6 ± 1.4	66.0 ± 2.7	80.1 ± 1.9	94.4 ± 2.6	180.32
2j	34.3 ± 1.7	48.2 ± 2.8	78.1 ± 1.9	92.3 ± 2.7	264.76
Acarbose	36.0 ± 2.5	50.4 ± 1.6	90.3 ± 2.2	94.5 ± 1.5	198.98

TABLE-4
ANTIDIABETIC EFFECT OF COMPOUNDS **2a-j** THROUGH α-AMYLASE INHIBITION ACTION

Compound	Inhibition rate (%)				IC_{50} (μM)
	125 μM	250 μM	500 μM	1000 μM	
2a	28.3 ± 1.7	47.0 ± 2.3	60.2 ± 1.8	76.4 ± 2.6	409.22
2b	40.5 ± 1.5	62.6 ± 2.4	73.9 ± 1.1	92.6 ± 2.4	141.46
2c	37.0 ± 0.8	49.6 ± 2.4	61.0 ± 1.8	89.7 ± 2.3	307.35
2d	44.9 ± 2.1	57.0 ± 1.3	73.3 ± 2.7	92.5 ± 0.6	145.53
2e	34.8 ± 2.2	56.9 ± 1.1	78.0 ± 2.4	92.8 ± 1.2	212.02
2f	26.0 ± 1.2	42.6 ± 0.4	72.7 ± 2.3	92.7 ± 1.3	354.17
2g	32.8 ± 2.2	46.7 ± 1.3	68.6 ± 0.4	84.9 ± 1.1	325.06
2h	37.2 ± 1.8	57.1 ± 2.9	89.0 ± 1.4	91.3 ± 2.7	146.58
2i	33.4 ± 2.6	57.0 ± 0.8	87.1 ± 2.9	91.1 ± 1.9	185.12
2j	32.7 ± 1.3	46.4 ± 2.6	78.6 ± 1.4	90.8 ± 2.2	283.00
Acarbose	30.7 ± 0.3	56.1 ± 1.9	85.0 ± 2.3	94.6 ± 1.4	220.83

The crystal structure of glucoamylase complexed with acarbose (PDB ID: 2F6D) was selected as the target for evaluating α-glucosidase inhibitory potential. Molecular docking of synthesised compounds **2a-j** and the reference drug acarbose with the 2F6D receptor was performed using AutoDock Vina. All synthesised derivatives displayed docking scores superior to that of acarbose (-7.4 kcal/mol). Compound **2b** exhibited the strongest binding affinity with a docking score of -10.0 kcal/mol, in agreement with its potent *in vitro* antidiabetic activity. Compound **2b** did not form hydrogen bond interactions within the active site; instead, its binding was stabilised through hydrophobic contacts involving Tyr63, Trp139, Glu210, Tyr351 and Glu456. In contrast, acarbose established eight hydrogen bond interactions with residues Tyr135 (2.65 and 2.24 Å), Glu211 (2.17 Å), Tyr63 (2.09 Å), Ala138 (3.26 Å), Asp70 (2.25 and 1.75 Å) and Arg345 (3.20 Å), together with hydrophobic interactions involving Tyr351, Glu210 and Trp139. Figs. 3 and 4 depict the hydrogen bond-

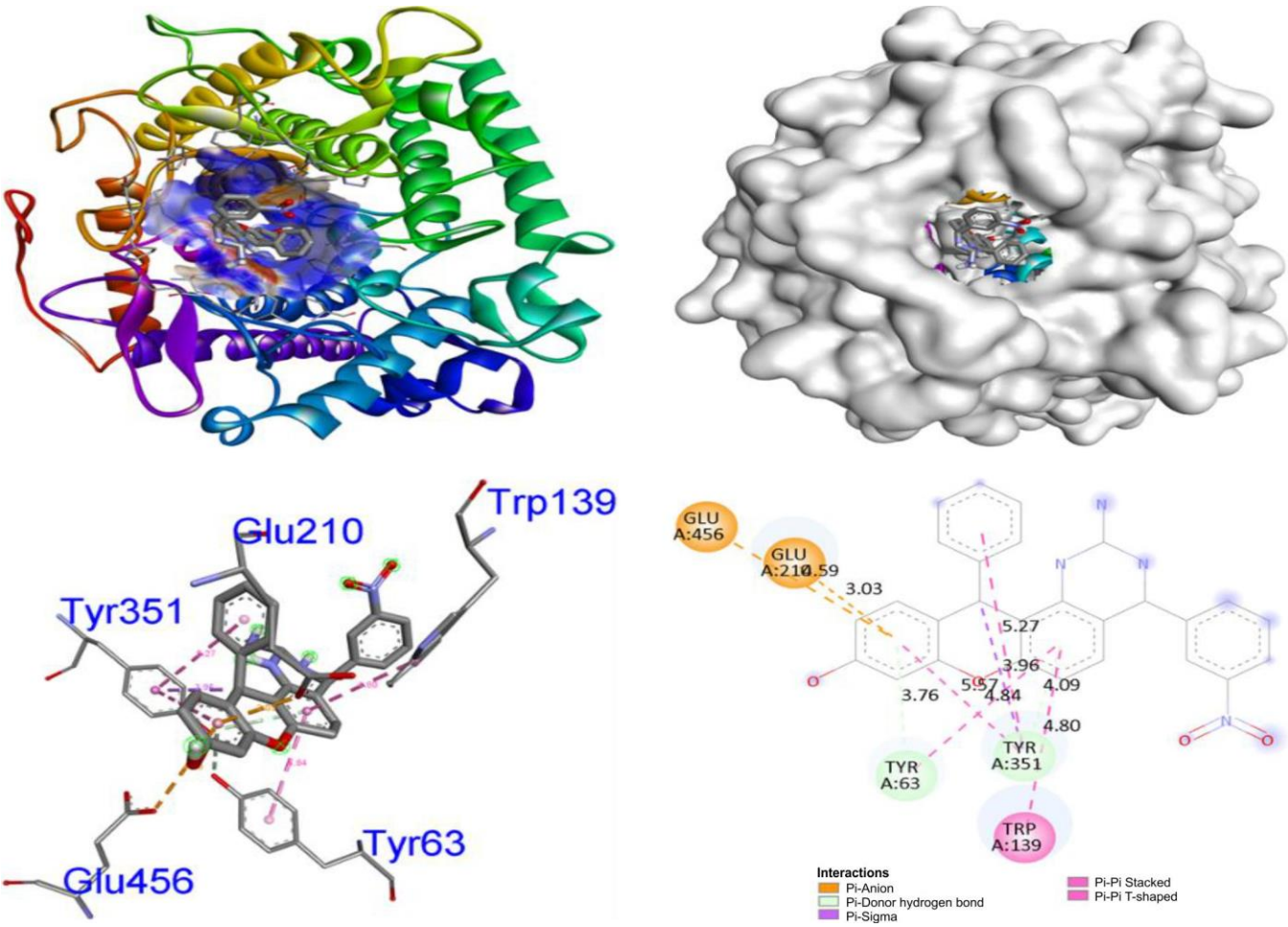

Fig. 3. Docked poses of inhibitor **2b** within the active region of 2F6D

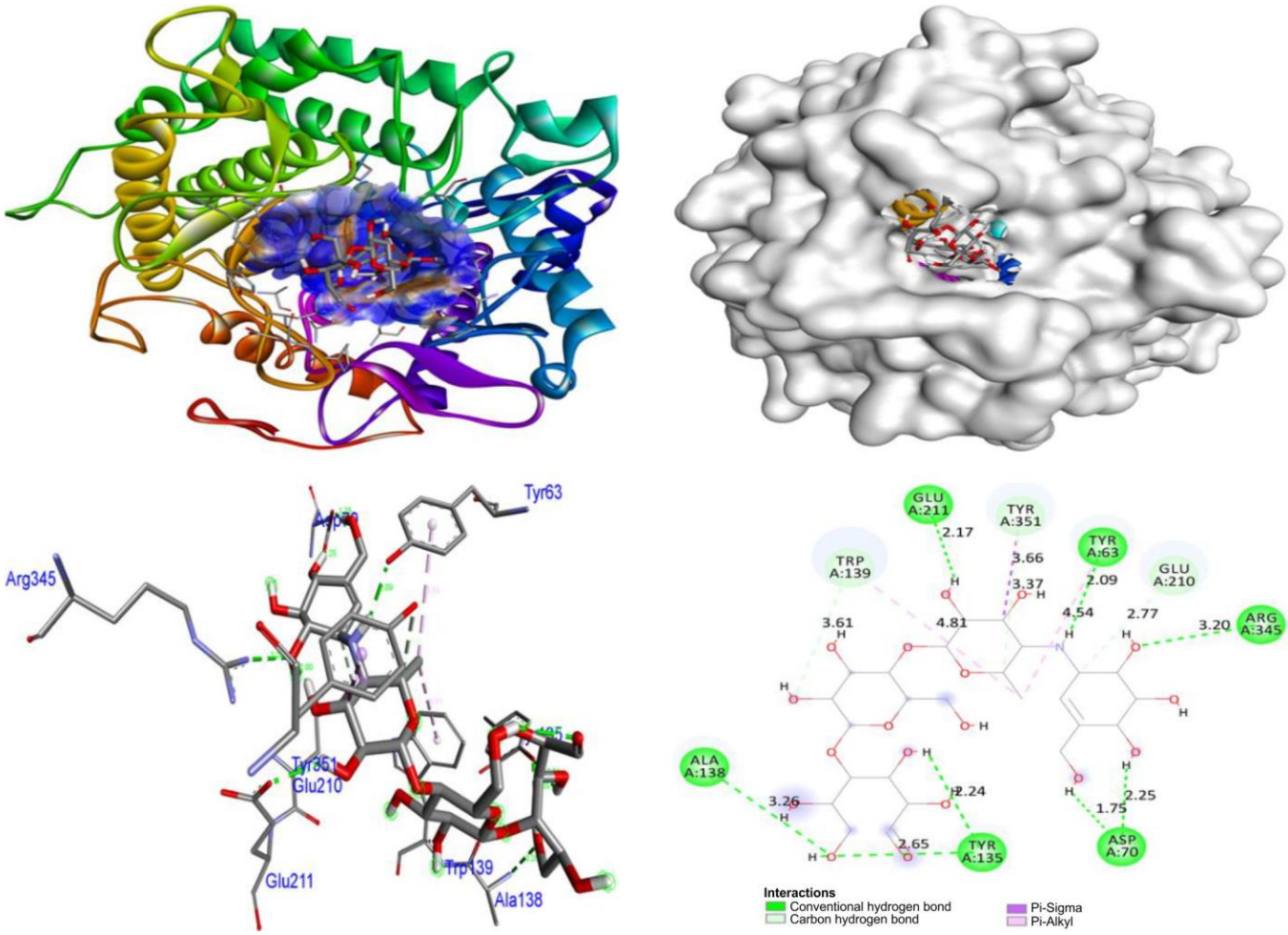

Fig. 4. Docked poses of control acarbose within the active region of 2F6D

ing and hydrophobic interaction profiles of compound **2b** and acarbose within the binding pocket of the 2F6D enzyme. The catalytic pocket of maltase-glucoamylase is known to involve residues such as Asp70, Glu210, Glu211 and Arg345 in ligand recognition and stabilisation, in agreement with the interaction pattern observed in the present study.

α-Amylase assay: This study employed the crystal structure of human pancreatic α-amylase complexed with nitrile and acarbose (PDB ID: 2QV4) for molecular docking studies. Compounds **2a-j** exhibited higher docking scores than the reference inhibitor acarbose, which displayed a binding affinity of -7.4 kcal/mol toward the 2QV4 receptor. Compound **2b** emerged as the most active derivative with a docking score of -9.7 kcal/mol and its binding affinity agreed with the *in vitro* α-amylase inhibitory results. Compound **2b** established four hydrogen bond interactions with residues Gln63, Asp300 and His305 at bond distances of 3.00, 2.36, 2.85 and 2.34 Å. Hydrophobic contacts involved residues Trp59, Leu162 and Ala198 which contributed to stabilisation of the ligand within the active site. Acarbose formed six hydrogen bond interactions with Thr162 (2.34 Å), Tyr62 (2.91 Å), Tyr151 (2.74 Å) and Glu233 (3.02, 2.66 and 2.31 Å). Hydrophobic interactions for acarbose involved residues His201, Asp300 and His305. Figs. 5 and 6 show the hydrogen bonding and hydrophobic interaction profiles of compound **2b** and acarbose within the binding cavity of the 2QV4 protein. Human pancreatic α-amylase possesses a well-defined catalytic region containing residues such as Asp300 and Glu233 that play essential roles in ligand recognition and enzyme inhibition.

Antioxidant: The crystal structure of the human antioxidant protein complexed with dithiothreitol (DTT) (PDB ID: 3MNG) was selected for antioxidant docking studies. The 3MNG structure corresponds to human peroxiredoxin V (PrxV) with DTT occupying the active site as a competitive inhibitor model. Molecular docking results revealed that compounds **2a-j** possessed binding affinities superior to that of ascorbic acid (-4.1 kcal/mol) within the 3MNG receptor. Compound **2b** exhibited the strongest interaction with a docking score of -6.4 kcal/mol relative to ascorbic acid. Compound **2b** did not participate in hydrogen bond formation within the active site. Stabilisation of the ligand was associated with hydrophobic contacts involving residues Pro40 Pro45 Gly46 and Cys47. Ascorbic acid established four hydrogen bond interactions with residues Thr44 at bond distances of 2.36 and 2.20 Å and Cys47 at bond distances of 4.12 and 2.79 Å. Hydrophobic interactions for ascorbic acid involved residue Thr147. Figs. 7 and 8 present the interaction profiles of compound **2b** and ascorbic acid within the 3MNG binding cavity.

The combined biological and computational results suggest that several members of the series possess promising

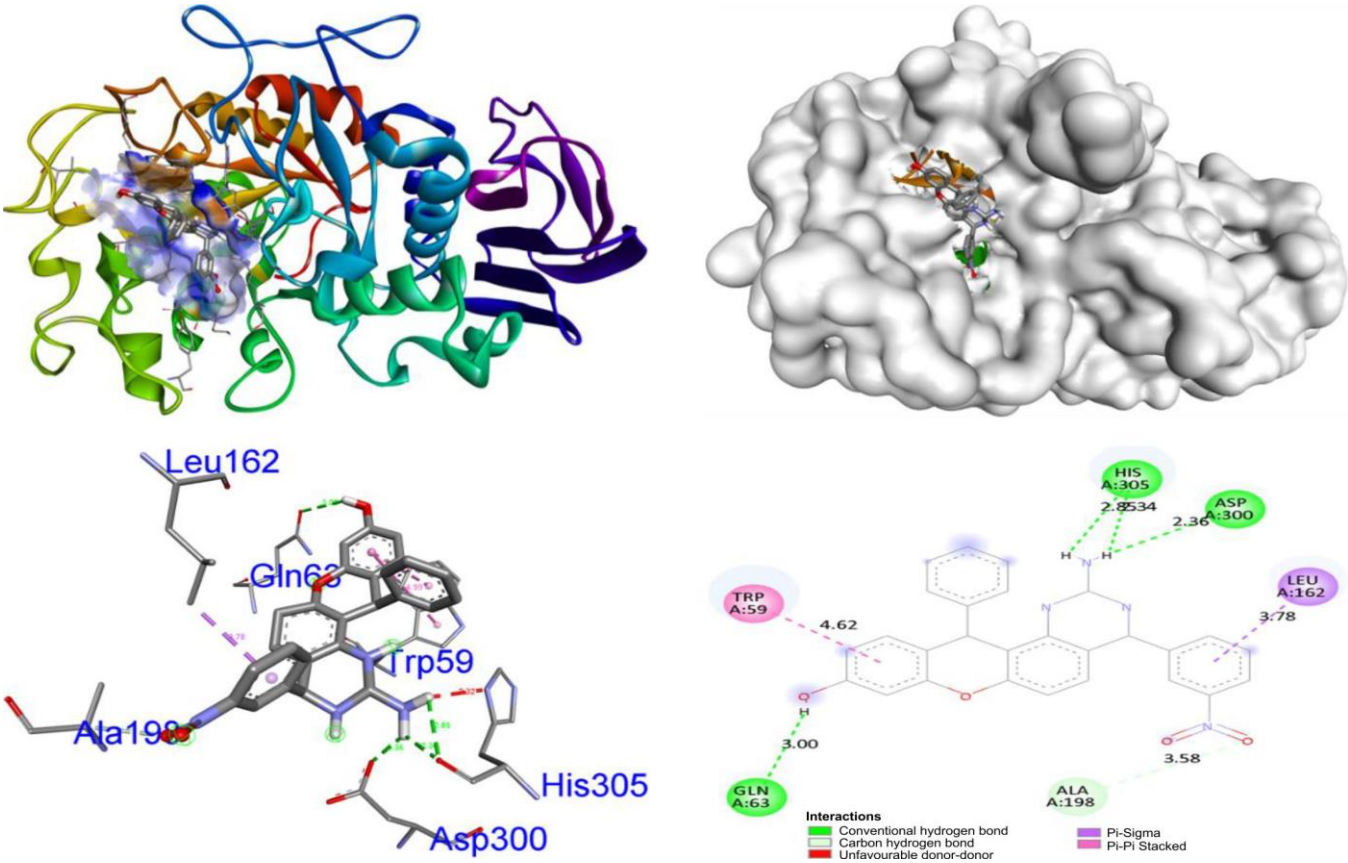

Fig. 5. Docked poses of inhibitor **2b** within the active region of 2QV4

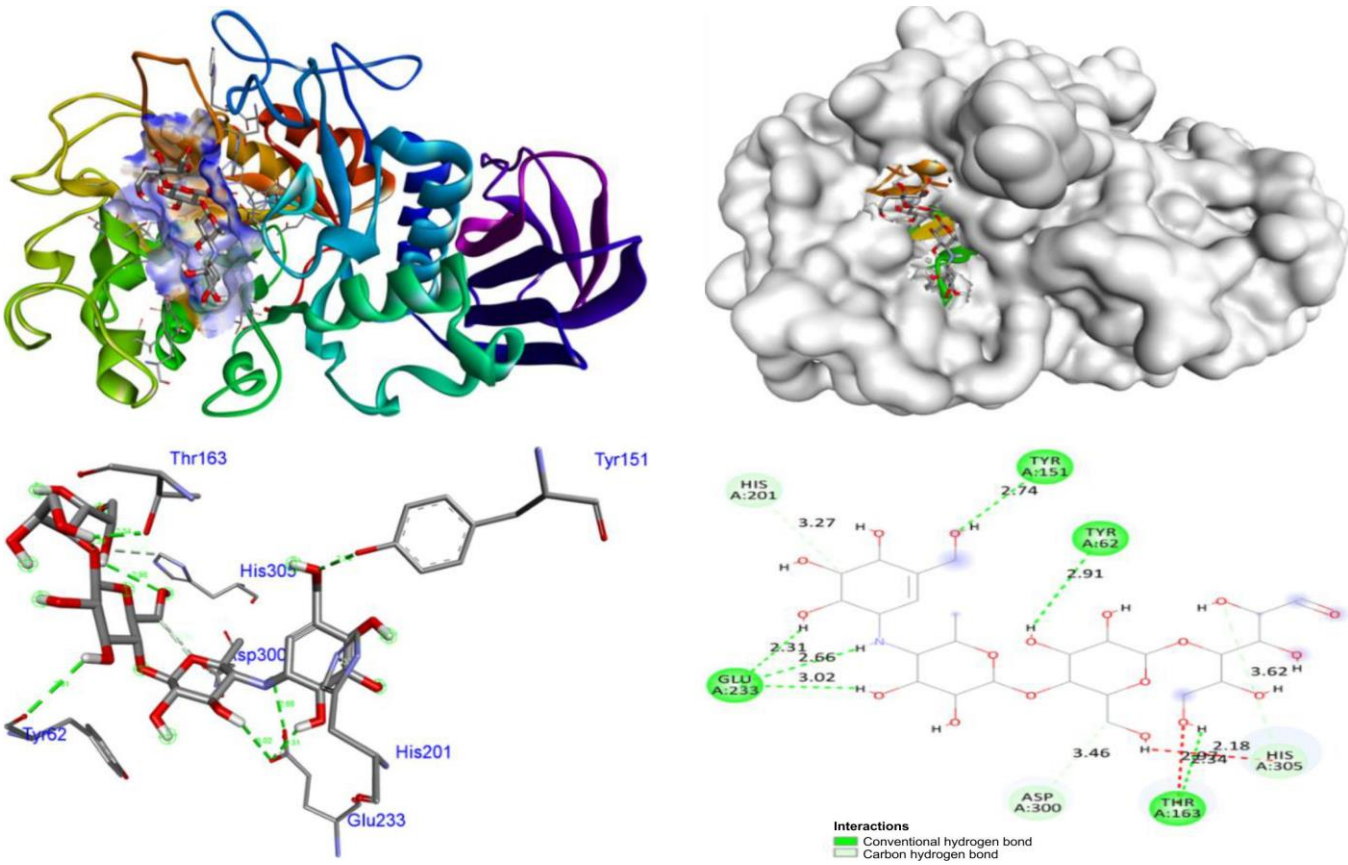

Fig. 6. Docked poses of control acarbose inside the active region of 2QV4

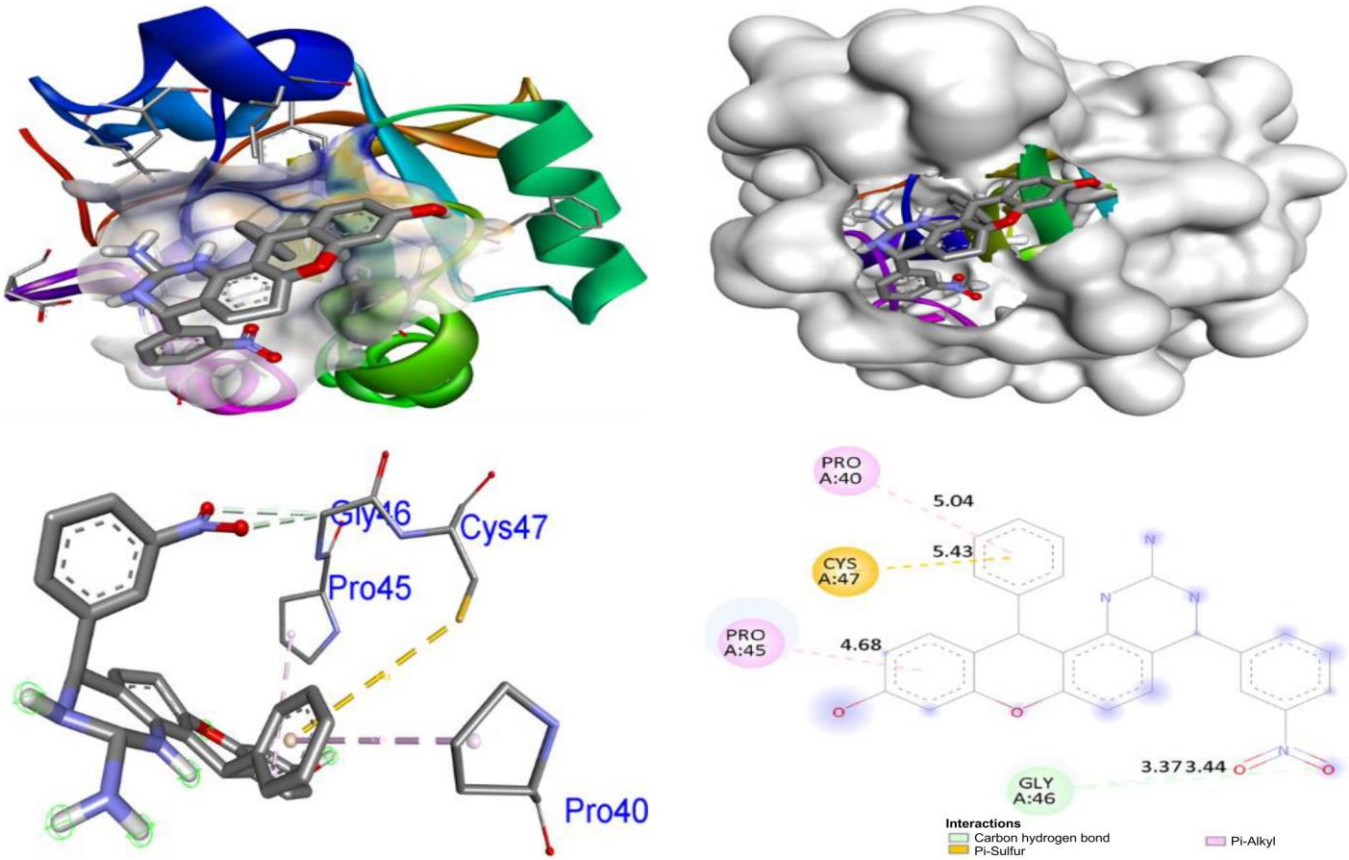

Fig. 7. Docked poses of inhibitor **2b** within the active region of 3MNG

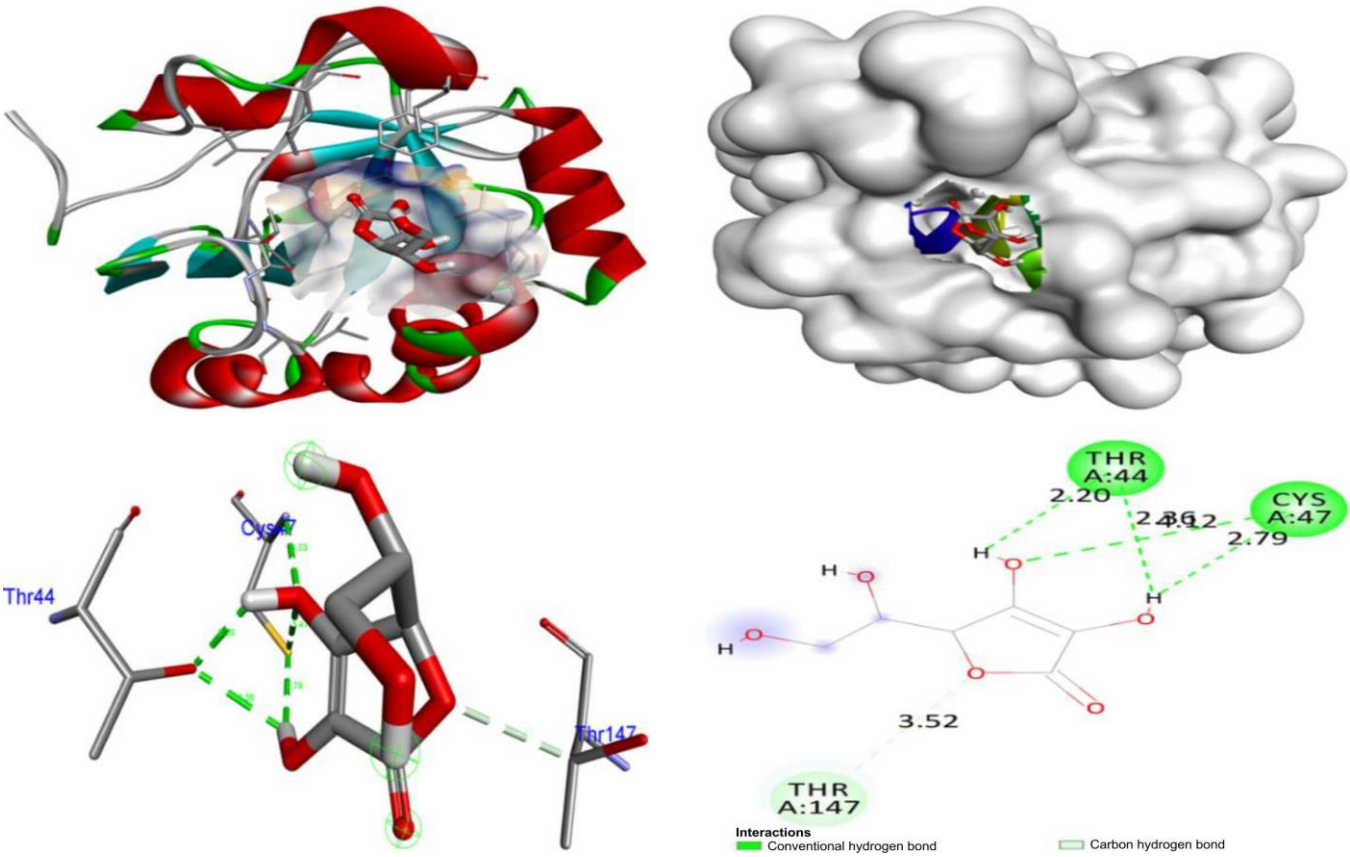

Fig. 8. Docked poses of control ascorbic acid within the active region of 3MNG

TABLE-5
INTERACTIONS OF COMPOUNDS **2a-j** AND CONTROL ACARBOSE TOWARDS 2F6D, 2QV4 AND 3MNG

Compounds	Docking score (kcal/mol)	Number of H-bonds	H-bonding residues (bond length, Å)
Glucoamylase (PDB ID: 2F6D)			
2a	-9.8	1	Tyr135 (3.18)
2b	-10.0	–	–
2c	-9.6	–	–
2d	-9.4	–	–
2e	-9.5	–	–
2f	-9.7	–	–
2g	-9.4	–	–
2h	-9.7	–	–
2i	-9.5	–	–
2j	-9.5	–	–
Acarbose	-7.4	8	Tyr63 (2.09), Asp70 (1.75 & 2.25), Tyr135 (2.24 & 2.65), Ala138 (3.26), Glu211 (2.17), Arg345 (3.20)
Human pancreatic α-amylase (PDB ID: 2QV4)			
2a	-8.5	1	Asp300 (2.28)
2b	-9.7	4	Gln63 (3.00), Asp300 (2.36), His305 (2.85 & 2.34)
2c	-9.1	1	Asp300 (2.46)
2d	-8.3	1	Asp300 (2.07)
2e	-8.4	–	–
2f	-8.5	2	Asp300 (2.56), His305 (2.74)
2g	-8.1	–	–
2h	-9.5	2	Thr163 (2.15), His305 (1.98)
2i	-8.1	1	Asp300 (2.28)
2j	-8.8	–	–
Acarbose	-7.4	6	Tyr62 (2.91), Tyr151 (2.74), Thr163 (2.34), Glu233 (2.31, 2.66 & 3.02)
Human antioxidant enzyme (PDB: 3MNG)			
2a	-5.0	1	Asp145 (2.96)
2b	-6.4	–	–
2c	-5.6	–	–
2d	-5.6	1	Thr147 (2.76)
2e	-4.8	–	–
2f	-5.0	3	Asn76 (3.38), Asp77 (2.00), Arg124 (3.21)
2g	-4.9	1	Arg124 (3.31)
2h	-5.3	2	Asp77 (2.03), Arg124 (3.31)
2i	-5.2	–	–
2j	-5.6	1	Thr147 (2.75)
Ascorbic acid	-4.1	4	Thr44 (2.20 & 2.36), Cys47 (2.12 & 2.79)

antioxidant and antidiabetic potential relative to the reference standards ascorbic acid and acarbose. A concise summary of the experimental and docking findings is provided in Table-5.

Conclusion

The novel pyrimido-xanthene analogues (**2a-j**) were synthesized using $FeSO_4 \cdot 7H_2O$ under solvent-free grinding conditions in good yields and short reaction times. $FeSO_4 \cdot 7H_2O$ proved to be an efficient catalyst for the one-pot three-component synthesis of pyrimido-xanthene derivatives. Structural elucidation of compounds **2a-j** was achieved using spectral techniques. Biological evaluation identified several derivatives with promising antioxidant and antidiabetic activities relative to ascorbic acid and acarbose. Molecular docking studies provided insight into ligand–target interactions associated with the observed biological responses. The combined experimental and computational findings suggest that pyrimido-xanthene derivatives represent an attractive scaffold for the development of new bioactive molecules.

CONFLICT OF INTEREST

The authors declare that there is no conflict of interests regarding the publication of this article.

DECLARATION OF AI-ASSISTED TECHNOLOGIES

During the preparation of this manuscript, the authors used an AI-assisted tool(s) to improve the language and no data, results or scientific conclusions were generated by AI. All analyses, interpretations and conclusions are the authors' own. The authors reviewed and edited the content and take full responsibility for the published work.

REFERENCES

1. M.J. Davies, D.A. D'Alessio, J. Fradkin, W.N. Kernan, C. Mathieu, G. Mingrone, P. Rossing, A. Tsapas, D.J. Wexler and J.B. Buse, *Diabetes Care*, **41**, 2669 (2018); https://doi.org/10.2337/dci18-0033

2. F. Bassyouni, M. Tarek, A. Salama, B. Ibrahim, S. Salah El Dine, N. Yassin, A. Hassanein, M. Moharam and M. Abdel-Rehim, *Molecules*, **26**, 2370 (2021); https://doi.org/10.3390/molecules26082370
3. B. Pandit and P. Saha, *Sustain. Chem. Climate Action*, **7**, 100140 (2025); https://doi.org/10.1016/j.scca.2025.100140
4. A. Selka, A. Abidli, L. Schiavo, L. Jeanmart, G. Hanquet and W.D. Lubell, *Eur. J. Org. Chem.*, **28**, e202400983 (2025); https://doi.org/10.1002/ejoc.202400983
5. R.M. Naidu Kalla, R.S. Karunakaran, M. Balaji and I. Kim, *ChemistrySelect*, **4**, 644 (2019); https://doi.org/10.1002/slct.201803449
6. M. Marinescu, *Molecules*, **26**, 6022 (2021); https://doi.org/10.3390/molecules26196022
7. Swati, Shaveta, Shalini, S. Sharma, R. Kumar, K. Kumar and V. Kumar, *Eur. J. Med. Chem.*, **302**, 118319 (2026); https://doi.org/10.1016/j.ejmech.2025.118319
8. G. Sanglikar and A.K. Tengli, *Results Chem.*, **15**, 102210 (2025); https://doi.org/10.1016/j.rechem.2025.102210
9. A. Kumar, A.K. Singh, H. Singh, V. Vijayan, D. Kumar, S. Thareja, J. Naik, J.P. Yadav, P. Pathak, M. Grishina, A. Verma, H. Khalilullah, M. Jaremko, A.-H. Emwas and P. Kumar, *Pharmaceuticals*, **16**, 299 (2023); https://doi.org/10.3390/ph16020299
10. T.A. Farghaly, M.F. Harras, A.M.R. Alsaedi, H.A. Thakir, H.K. Mahmoud and D.F. Katowah, *Mini Rev. Med. Chem.*, **23**, 821 (2023); https://doi.org/10.2174/1389557523666221220142911
11. B.J.H. Uhlenbruck, C.M. Josephitis, L. de Lescure, R.S. Paton and A. McNally, *Nature*, **631**, 87 (2024); https://doi.org/10.1038/s41586-024-07474-1
12. B. Nammalwar and R.A. Bunce, *Pharmaceuticals*, **17**, 104 (2024); https://doi.org/10.3390/ph17010104
13. Y. Li, T. Tan, Y. Zhao, Y. Wei, D. Wang, R. Chen and L. Tao, *ACS Macro Lett.*, **9**, 1249 (2020); https://doi.org/10.1021/acsmacrolett.0c00496
14. J. Bais, F. Benedetti, F. Berti, I. Cerminara, S. Drioli, M. Funicello, G. Regini, M. Vidali and F. Felluga, *Molecules*, **25**, 4152 (2020); https://doi.org/10.3390/molecules25184152
15. A. Kapri, S. Pant, N. Gupta and S. Nain, *Pharm. Chem. J.*, **56**, 461 (2022); https://doi.org/10.1007/s11094-022-02661-8
16. A. Chaudhary and J.M. Khurana, *Curr. Org. Synth.*, **15**, 341 (2018); https://doi.org/10.2174/1570179414666171011162902
17. M. Maia, D.I.S.P. Resende, F. Durães, M.M.M. Pinto and E. Sousa, *Eur. J. Med. Chem.*, **210**, 113085 (2021); https://doi.org/10.1016/j.ejmech.2020.113085
18. K. Selvaraj, V. Loganathan, A. Ahamed, A. A. Hatamleh, A. Manilal, and I. Akbar, *J. Mol. Struct.*, **1329**, 141447 (2025); https://doi.org/10.1016/j.molstruc.2025.141447
19. T. Dutta, T. Das, A.V. Gopalakrishnan, S.C. Saha, M. Ghorai, S. Nandy, M. Kumar, R. Radha, A. Ghosh, N. Mukerjee and A. Dey, *Naunyn Schmiedebergs Arch. Pharmacol.*, **396**, 851 (2023); https://doi.org/10.1007/s00210-022-02373-6
20. L.M. Aroua, H.R. Almuhaylan, F.M. Alminderej, S. Messaoudi, S. Chigurupati, S. Al-Mahmoud and H.A. Mohammed, *Bioorg. Chem.*, **114**, 105073 (2021); https://doi.org/10.1016/j.bioorg.2021.105073
21. I.F.F. Benzie and J.J. Strain, *Anal. Biochem.*, **239**, 70 (1996); https://doi.org/10.1006/abio.1996.0292
22. A.E. Martin and P.A. Montgomery, *Am. J. Health Syst. Pharm.*, **53**, 2277 (1996); https://doi.org/10.1093/ajhp/53.19.2277
23. S. Yousuf, K.M. Khan, U. Salar, S. Chigurupati, M.T. Muhammad, A. Wadood, M. Aldubayan, V. Vijayan, M. Riaz and S. Perveen, *Eur. J. Med. Chem.*, **159**, 47 (2018); https://doi.org/10.1016/j.ejmech.2018.09.052
24. F. Saleem, Kanwal, K.M. Khan, S. Chigurupati, M. Solangi, A.R. Nemala, M. Mushtaq, Z. Ul-Haq, M. Taha and S. Perveen, *Bioorg. Chem.*, **106**, 104489 (2021); https://doi.org/10.1016/j.bioorg.2020.104489
25. G.M. Morris, R. Huey and A.J. Olson, *Curr. Protoc. Bioinformatics*, **24**, 8 (2008); https://doi.org/10.1002/0471250953.bi0814s24
26. K. Mseddi, F. Alimi, E. Noumi, V.N. Veettil, S. Deshpande, M. Adnan, A. Hamdi, S. Elkahoui, A. Alghamdi, A. Kadri, M. Patel and M. Snoussi, *Arab. J. Chem.*, **13**, 6782 (2020); https://doi.org/10.1016/j.arabjc.2020.06.032
27. A. Pedretti, L. Villa and G. Vistoli, *J. Comput. Aided Mol. Des.*, **18**, 167 (2004); https://doi.org/10.1023/B:JCAM.0000035186.90683.f2
28. O. Trott and A.J. Olson, *J. Comput. Chem.*, **31**, 455 (2010); https://doi.org/10.1002/jcc.21334
29. R.M.N. Kalla, R.S. Karunakaran, M. Balaji and I. Kim, *ChemistrySelect*, **4**, 644 (2019); https://doi.org/10.1002/slct.201803449
30. BIOVIA Dassault Systems, BIOVIA Discovery Studio Visualizer; v16.1.0.15350; Dassault Systems: San Diego, USA (2015).